RNA Mimics of Green Fluorescent Protein

Jeremy S. Paige, *et al.*

Science **333**, 642 (2011);
DOI: 10.1126/science.1207339

the leading cause of death in children between 1 month and 1 year of age (*21*), multiple abnormalities in the brainstem serotonergic system have been identified, including serotonin insufficiency (*20*, *21*). Our findings suggest that such insufficiency might compromise an infant's respiratory response to hypercapnic acidosis that may occur upon rebreathing exhaled air as a result of sleeping prone in the face-down position (SIDS infants are often found prone), contributing to respiratory failure and death. By contrast, serotonin syndrome is a disorder of serotonin excess and extreme hyperthermia, shivering, seizures, coma, and in some cases death that can result acutely from serotonin drug interactions (*22*). This association between serotonin excess and hyperthermia is consistent with our reciprocal findings of serotonergic inhibition inducing hypothermia. We presume that in vivo CNO/Di signaling suppresses action potential firing, resulting in net inhibition of serotonergic neuron activity. Other scenarios are possible, such as net excitation, but seem improbable given the whole-animal phenotypes observed upon CNO/Di signaling in serotonergic neurons, the molecular mechanism by which Di appears to act, and the paucity of evidence that net excitation could occur. For example, such net excitation has not been observed in cultured serotonergic neurons, nor in extensive studies on 5HT1A receptor agonists in vivo or ex vivo, which act mechanistically like CNO/Di (*37*, *38*). Assessing the precise in vivo electrophysiological effects of CNO/Di signaling on serotonergic neuron activity, including chemoresponsiveness, awaits the means to record from individual medullary serotonergic neurons over the course of hours (see Fig. 3E) in unanesthetized, conscious mice. By contrast, recordings made during either anesthesia (*15*, *39*–*41*) or decerebration (*42*, *43*) suffer from the confound of perturbing serotonergic neuron activity and chemoreflex properties—the very processes under examination.

The present studies, as well as our analyses of broad constitutive Di expression and activity (fig. S4), establish *RC::FPDi* as a neuronal perturbation tool featuring in vivo ligand inducibility within seconds to minutes, inhibition for minutes to hours, reversibility within hours, intra-animal repeatability, and high cell-subtype selectivity (including anatomically dispersed populations) and thus resolution for functional mapping. This tool can be applied in the awake, freely behaving animal without confounding interference from anesthesia, surgical procedures such as cannulation, or compensatory changes in circuitry that can develop in response to constitutive genetic alterations. *RC::FPDi* can be applied to map other behaviors in which dysregulation of specific populations has been implicated.

References and Notes

1. I. R. Leusen, *Am. J. Physiol.* **176**, 39 (1954).
2. S. S. Kety, R. E. Forster, *Biogr. Mem. Natl. Acad. Sci.* **79**, 66 (2001).
3. E. Nattie, *J. Appl. Physiol.* **110**, 1 (2011).
4. P. G. Guyenet, R. L. Stornetta, D. A. Bayliss, *J. Comp. Neurol.* **518**, 3883 (2010).
5. C. A. Smith, J. R. Rodman, B. J. Chenuel, K. S. Henderson, J. A. Dempsey, *J. Appl. Physiol.* **100**, 13 (2006).
6. J. S. Haldane, J. G. Priestley, *J. Physiol.* **32**, 225 (1905).
7. R. A. Mitchell, H. H. Loeschcke, W. H. Massion, J. W. Severinghaus, *J. Appl. Physiol.* **18**, 523 (1963).
8. M. Elam, T. Yao, P. Thorén, T. H. Svensson, *Brain Res.* **222**, 373 (1981).
9. R. H. Williams, L. T. Jensen, A. Verkhratsky, L. Fugger, D. Burdakov, *Proc. Natl. Acad. Sci. U.S.A.* **104**, 10685 (2007).
10. A. Li, L. Emond, E. Nattie, *Adv. Exp. Med. Biol.* **605**, 371 (2008).
11. A. V. Gourine *et al.*, *Science* **329**, 571 (2010).
12. A. E. Corcoran *et al.*, *Respir. Physiol. Neurobiol.* **168**, 49 (2009).
13. G. B. Richerson, *J. Neurophysiol.* **73**, 933 (1995).
14. M. R. Hodges, G. B. Richerson, *J. Appl. Physiol.* **108**, 1425 (2010).
15. S. D. Depuy, R. Kanbar, M. B. Coates, R. L. Stornetta, P. G. Guyenet, *J. Neurosci.* **31**, 1981 (2011).
16. W. Wang, G. B. Richerson, *Neuroscience* **90**, 1001 (1999).
17. S. F. Morrison, K. Nakamura, C. J. Madden, *Exp. Physiol.* **93**, 773 (2008).
18. M. R. Hodges *et al.*, *J. Neurosci.* **28**, 2495 (2008).
19. G. Cano *et al.*, *J. Comp. Neurol.* **460**, 303 (2003).
20. J. R. Duncan *et al.*, *JAMA* **303**, 430 (2010).
21. H. C. Kinney, G. B. Richerson, S. M. Dymecki, R. A. Darnall, E. E. Nattie, *Annu. Rev. Pathol.* **4**, 517 (2009).
22. H. Sternbach, *Am. J. Psychiatry* **148**, 705 (1991).
23. R. Awatramani, P. Soriano, C. Rodriguez, J. J. Mai, S. M. Dymecki, *Nat. Genet.* **35**, 70 (2003).
24. P. Jensen *et al.*, *Nat. Neurosci.* **11**, 417 (2008).
25. J. C. Kim *et al.*, *Neuron* **63**, 305 (2009).
26. B. N. Armbruster, X. Li, M. H. Pausch, S. Herlitze, B. L. Roth, *Proc. Natl. Acad. Sci. U.S.A.* **104**, 5163 (2007).
27. M. D. Mark, S. Herlitze, *Eur. J. Biochem.* **267**, 5830 (2000).
28. S. M. Ferguson *et al.*, *Nat. Neurosci.* **14**, 22 (2011).
29. S. M. Dymecki, J. C. Kim, *Neuron* **54**, 17 (2007).
30. N. J. Penington, J. S. Kelly, A. P. Fox, *J. Physiol.* **469**, 387 (1993).
31. P. Bonnavion, J. F. Bernard, M. Hamon, J. Adrien, V. Fabre, *J. Comp. Neurol.* **518**, 2744 (2010).
32. W. Wang, J. H. Pizzonia, G. B. Richerson, *J. Physiol.* **511**, 433 (1998).
33. M. B. Dias, A. Li, E. Nattie, *J. Appl. Physiol.* **105**, 83 (2008).
34. V. Dubreuil *et al.*, *J. Neurosci.* **29**, 14836 (2009).
35. N. Marina *et al.*, *J. Neurosci.* **30**, 12466 (2010).
36. I. C. Wenker, O. Kréneisz, A. Nishiyama, D. K. Mulkey, *J. Neurophysiol.* **104**, 3042 (2010).
37. G. Piñeyro, P. Blier, *Pharmacol. Rev.* **51**, 533 (1999).
38. R. B. Innis, G. K. Aghajanian, *Eur. J. Pharmacol.* **143**, 195 (1987).
39. G. Gobbi *et al.*, *Eur. Neuropsychopharmacol.* **17**, 328 (2007).
40. A. J. Patel *et al.*, *Nat. Neurosci.* **2**, 422 (1999).
41. C. P. Washburn, J. E. Sirois, E. M. Talley, P. G. Guyenet, D. A. Bayliss, *J. Neurosci.* **22**, 1256 (2002).
42. F. Hayashi, J. D. Sinclair, *Respir. Physiol.* **84**, 61 (1991).
43. W. M. St-John, J. F. Paton, *Respir. Physiol.* **123**, 201 (2000).

Acknowledgments: Supported by NIH grants F32HD063257-01A1 (R.R.), 5R21DA023643-02 (R.B., S.D.), 5R21MH083613-02 (R.R., J.C.K., S.D.), 5P01HD036379-13 (R.R., A.C., R.B., J.C.K., E.N., G.R., S.D.), 5R01HL028066-30 (A.C., E.N.), and 5R01HD052772 (G.R.). Clozapine-*N*-oxide used in some preliminary experiments was provided through the NIH Rapid Access to Intervention Development Program. We thank B. Roth for providing the Di-encoding cDNA; B. Roth, W. Regehr, C. Hull, B. Sabatini, and members of the Dymecki lab for helpful discussions; and Y. Wu and J. J. Mai for technical assistance. The authors declare no conflicts of interest.

Supporting Online Material

www.sciencemag.org/cgi/content/full/333/6042/637/DC1
Materials and Methods
Figs. S1 to S4
References (*44*–*53*)

7 March 2011; accepted 15 June 2011
10.1126/science.1205295

RNA Mimics of Green Fluorescent Protein

Jeremy S. Paige,[1] Karen Y. Wu,[1] Samie R. Jaffrey[1,2]*

Green fluorescent protein (GFP) and its derivatives have transformed the use and analysis of proteins for diverse applications. Like proteins, RNA has complex roles in cellular function and is increasingly used for various applications, but a comparable approach for fluorescently tagging RNA is lacking. Here, we describe the generation of RNA aptamers that bind fluorophores resembling the fluorophore in GFP. These RNA-fluorophore complexes create a palette that spans the visible spectrum. An RNA-fluorophore complex, termed Spinach, resembles enhanced GFP and emits a green fluorescence comparable in brightness with fluorescent proteins. Spinach is markedly resistant to photobleaching, and Spinach fusion RNAs can be imaged in living cells. These RNA mimics of GFP provide an approach for genetic encoding of fluorescent RNAs.

The fluorophore in green fluorescent protein (GFP) is formed from three residues in the nascent protein, Ser^{65}-Tyr^{66}-Gly^{67}, that undergo an autocatalytic intramolecular cyclization. The resulting fluorophore, 4-hydroxybenzlidene imidazolinone (HBI) (Fig. 1A), is encased within the protein, enabling its fluorescence (*1*). Chemically synthesized HBI is nonfluorescent (*2*), as is denatured GFP (*3*). However, upon refolding, the fluorescence of GFP is recovered (*3*). The folded GFP protein forms specific contacts with the fluorophore that prevent intramolecular motions, making fluorescence the major pathway available to dissipate the energy of the excited state fluorophore (*4*).

The ability to confer GFP-like functionality to RNA would facilitate studies of RNA biology and advance RNA-based applications. An RNA sequence with GFP-like properties should exhibit

[1]Department of Pharmacology, Weill Medical College, Cornell University, New York, NY 10065, USA. [2]Tri-Institutional Program in Chemical Biology, Weill Medical College, Cornell University, New York, NY 10065, USA.

*To whom correspondence should be addressed. E-mail: srj2003@med.cornell.edu

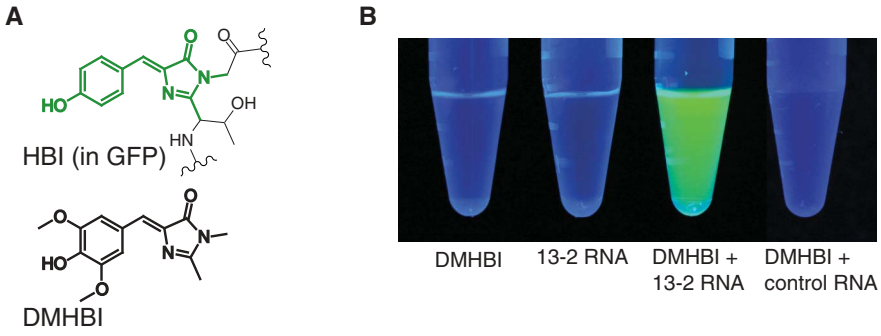

Fig. 1. RNA aptamers switch on the fluorescence of GFP-like fluorophores. (**A**) Structures of HBI (green), in the context of GFP, and DMHBI. (**B**) 13-2 enhances the fluorescence of DMHBI. Solutions containing DMHBI, 13-2 RNA, DMHBI with 13-2 RNA, or DMHBI with total HeLa cell RNA were photographed under illumination with 365 nm of light. The image is a montage obtained under identical image-acquisition conditions.

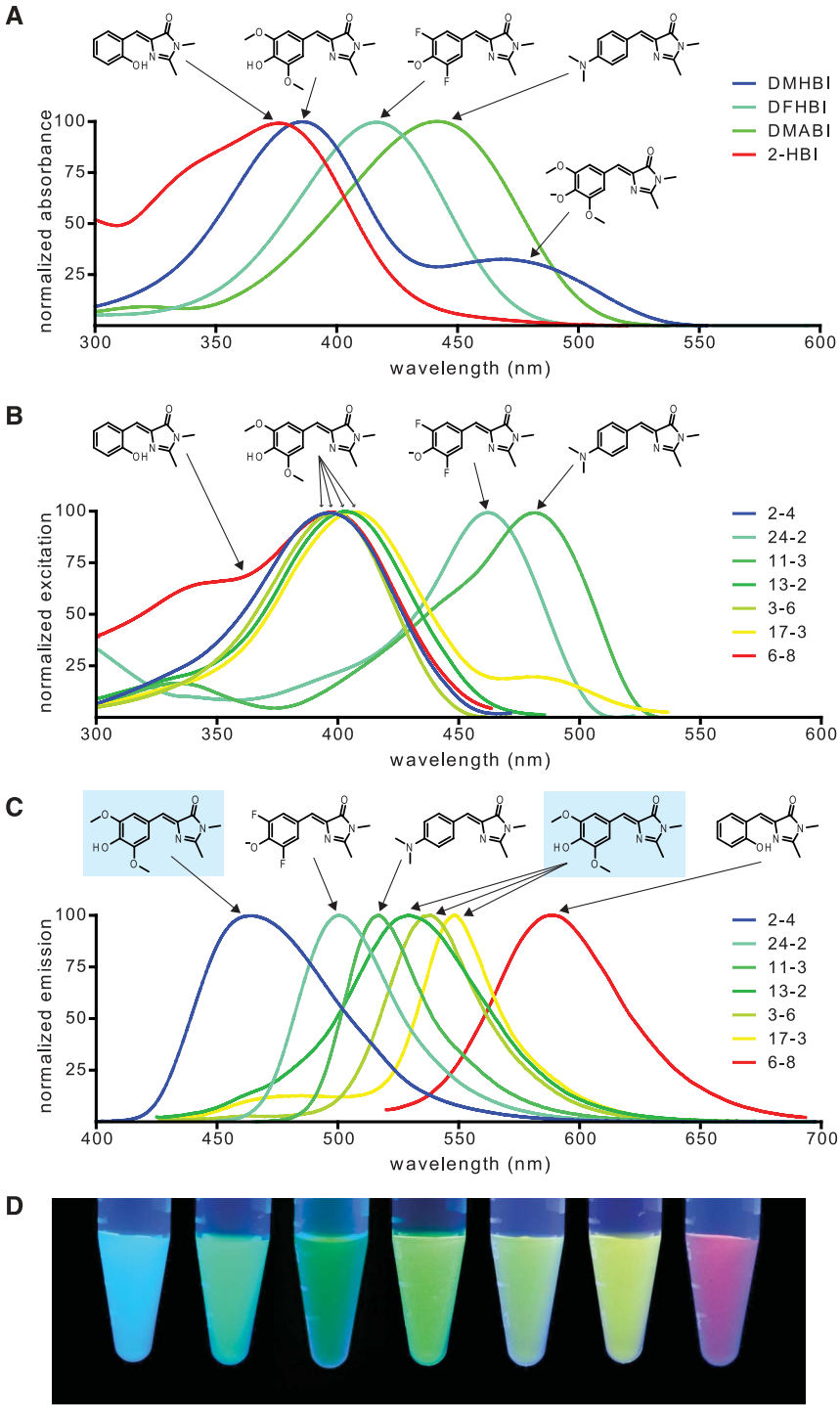

Fig. 2. Spectral tuning and fluorophore diversity produce a palette of RNA-fluorophore complexes. (**A**) Absorbance spectra of GFP-like fluorophores. Spectra were collected in the absence of RNA at pH 7.4. (**B** and **C**) Excitation (B) and emission (C) spectra of RNA-fluorophore complexes. Spectra were collected in the presence of excess fluorophore at pH 7.4 for RNAs binding to DMHBI (2-4, 13-2, 3-6, and 17-3), DFHBI (24-2), DMABI (11-3), and 2-HBI (6-8). Spectra are normalized to the excitation and emission peak for each complex. Arrows indicate the fluorophore from which each spectrum is derived. For emission spectra (C), DMHBI is indicated with blue shading. (**D**) RNA-fluorophore complexes were illuminated with ultraviolet light (365 nm) and photographed. From left to right, the tubes contain RNAs 2-4, 24-2, 11-3, 13-2, 3-6, 17-3, 6-8, and fluorophores as indicated above. The image is a montage obtained under identical image-acquisition conditions.

fluorescence upon binding a small-molecule fluorophore. However, in order to have fluorescence only associated with the RNA, the small molecule would need to be in a nonfluorescent form when not bound and switch to a fluorescent form only when bound. Antibodies and aptamers capable of eliciting the fluorescence of conditionally fluorescent dyes have been described (*5*–*7*). However, most conditional fluorophores can also be activated nonspecifically (*4*) or have other undesirable properties such as cytotoxicity (*8*) [supporting online material (SOM) text]. We therefore sought to identify a small molecule whose fluorescence could be activated by a specific RNA sequence yet not activated by other cellular constituents.

Because fluorescence enhancement of HBI requires suppression of subtle movements of the fluorophore (*4*), we reasoned that the fluorescence of HBI would not be induced by cellular constituents. To test this, we prepared several HBI derivatives (fig. S1A) and found that these compounds were not detectably fluorescent upon incubation with cells (fig. S1B) or cellular RNA or DNA (fig. S1C). Incubation of GFP-like fluorophores with cells illuminated for 10 min at 37°C resulted in negligible cell death, whereas another conditional fluorophore, malachite green, exhibited considerable cytotoxicity (fig. S1D).

We next sought to identify RNA sequences that bind and activate the fluorescence of GFP fluorophores, beginning with 3,5-dimethoxy-4-hydroxybenzylidene imidazolinone (DMHBI) (Fig. 1A). We performed systematic evolution of ligands by exponential enrichment (SELEX) (*9*, *10*) with a library containing ~5×10^{13} RNA molecules and selected RNAs for their ability to bind DMHBI-agarose. After five rounds of selection, the pool of RNAs weakly activated DMHBI fluorescence, with further increases in fluorescence up to round 10 (fig. S2A).

To identify individual RNA aptamers that accounted for DMHBI fluorescence, we screened individual sequences and identified one RNA, 13-2 (fig. S2, B and C), which exhibited the highest degree of aptamer-induced fluorescence (Fig. 1B). The spectra of the 13-2-DMHBI complex contained a single emission peak at 529 nm and single excitation peak at 398 nm (fig. S2B). The brightness of 13-2-DMHBI was 12% relative to GFP (table S1), and the dissociation constant (K_d) for the 13-2-DMHBI complex is 464 nM (fig. S2D). Truncation and mutagenesis experiments supported the secondary structure predicted by Mfold (fig. S2E) (*11*) and resulted in a 60-nucleotide (nt) minimal domain with enhanced quantum yield (table S1 and fig. S2E).

To determine whether DMHBI could be spectrally tuned with RNA to exhibit a range of fluorescence properties, we performed further SELEX screens (*12*). Several aptamers were identified that exhibited markedly different spectral properties, including light blue (2-4), greenish-yellow (3-6), and yellow (17-3) fluorescence (Fig. 2, A to D, and table S1). Sequence alignment of these aptamers reveals little sequence similarity, and secondary structure analysis predicts a range of structures (fig. S3).

To further extend spectral properties, we generated two additional GFP-like fluorophores, 4-dimethylaminobenzylidene imidazolinone (DMABI) and 2-hydroxybenzlidene imidazolinone (2-HBI) (fig. S1A). An aptamer selected against DMABI exhibited green fluorescence, whereas an aptamer selected against 2-HBI exhibited orange-red fluorescence (Fig. 2D and fig. S3). Thus, a range of RNA-fluorophore complexes spanning the visible spectrum can be generated by using GFP-like fluorophores.

A major advance in GFP technology was the discovery of enhanced GFP (EGFP) (*13*). The HBI fluorophore in GFP/EGFP can exist in either the phenol (protonated) or phenolate (deprotonated) form. In GFP, the phenol form predominates at neutral pH because of the relatively high pK_a (where K_a is the acid dissociation constant) of HBI (*14*), whereas in EGFP, HBI is almost exclusively in the phenolate form (*13*). The phenolate species exhibits a higher extinction coefficient, which contributes to the increased brightness of EGFP (*13*).

Characterization of the DMHBI-binding aptamers suggested that these complexes mimic GFP rather than EGFP. Like HBI, DMHBI at pH 7.4 is primarily in the phenol form, with a small portion in the phenolate form (Fig. 2A), which is consistent with its pK_a of 8.0 (fig. S4A). When bound to 17-3, the excitation spectrum reveals both forms, indicating that this aptamer binds DMHBI irrespective of its protonation state (Fig. 2B). Thus, the 17-3–DMHBI complex most closely resembles GFP. In contrast, when DMHBI is bound to either 13-2, 2-4, or 3-6 the excitation spectra reveals that RNA binds exclusively to the phenolic form of the fluorophore (Fig. 2B).

To generate RNA-fluorophore complexes that exhibit the spectral properties of EGFP, we used a biomimetic strategy to obtain RNAs that bind the phenolate form of a GFP-like fluorophore. We designed a new HBI derivative, 3,5-difluoro-4-hydroxybenzylidene imidazolinone (DFHBI), which is exclusively in the phenolate form because of the introduction of fluorine residues that reduce the pK_a (Fig. 2A). An aptamer selected against DFHBI (24-2) exhibited an excitation spectra that is consistent with exclusive binding to the phenolate form of DFHBI (Fig. 3A) and a markedly enhanced quantum yield of

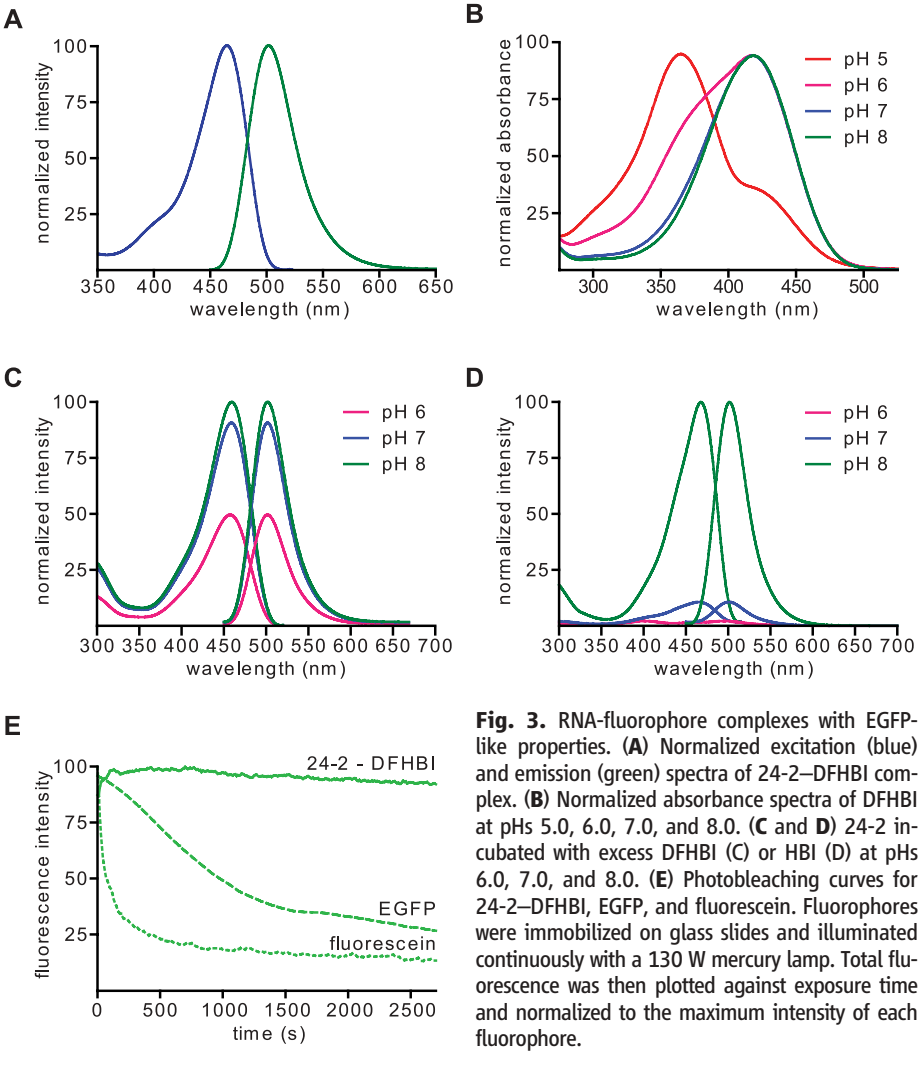

Fig. 3. RNA-fluorophore complexes with EGFP-like properties. (**A**) Normalized excitation (blue) and emission (green) spectra of 24-2–DFHBI complex. (**B**) Normalized absorbance spectra of DFHBI at pHs 5.0, 6.0, 7.0, and 8.0. (**C** and **D**) 24-2 incubated with excess DFHBI (C) or HBI (D) at pHs 6.0, 7.0, and 8.0. (**E**) Photobleaching curves for 24-2–DFHBI, EGFP, and fluorescein. Fluorophores were immobilized on glass slides and illuminated continuously with a 130 W mercury lamp. Total fluorescence was then plotted against exposure time and normalized to the maximum intensity of each fluorophore.

0.72, which is 20% higher than EGFP (table S1). The molar brightness of 24-2–DFHBI is 53% of EGFP but brighter than many other fluorescent proteins (table S1) (*15*).

To determine whether 24-2 selectively recognizes the phenolate form of DFHBI, we measured its spectral properties at different pHs. When the pH is lowered to pH 6.0, both the phenolic and phenolate forms of DFHBI are detected (Fig. 3B). However, at pH 6.0, the 24-2–DFHBI complex exhibits only the phenolate excitation peak, indicating preferential binding of the RNA to the phenolate form of the fluorophore (Fig. 3C). We also examined the binding of 24-2 to HBI, which resembles DFHBI but lacks fluorines. 24-2 weakly binds and activates the fluorescence of HBI at pH 8.0, at which both the phenol and phenolate forms are present (*16*). However, at pH 7.0 and 6.0, at which only the phenol form is present, 24-2 fails to activate HBI fluorescence. Taken together, these data suggest that 24-2 selectively recognizes the phenolate form of the fluorophore.

We next examined the photobleaching properties of 24-2–DFHBI complexes. 24-2 was immobilized to a glass surface, and total fluorescence was measured with DFHBI in solution over 45 min of continuous illumination. Compared with fluorescein and EGFP, 24-2–DFHBI exhibited negligible photobleaching, suggesting that exchange of bound DFHBI with DFHBI in solution prevents the accumulation of photobleached complexes.

Because of the green fluorescence and useful spectral properties of 24-2–DFHBI complexes, we termed the 24-2 sequence "Spinach." To examine Spinach fluorescence in cells, we transformed *Escherichia coli* with plasmids expressing Spinach fused to a short RNA-stabilizing element (*17*). After a brief incubation with DFHBI, we found that fluorescence was readily detectable in individual cells (fig. S5A) as well as in colonies on a plate (fig. S5B).

To determine whether Spinach could be used to tag RNAs in living mammalian cells, we fused Spinach to the 3′ end of 5*S* (fig. S6), a small noncoding RNA transcribed by RNA polymerase III (Pol III) that associates with the large ribosomal subunit, and transfected this construct into human embryonic kidney (HEK) 293 T cells. The 3′ end of 5*S* is solvent-exposed, and addition of short sequences to the 3′ end does not affect 5*S* localization (*18*). 5*S*-Spinach fluorescence was detected throughout cells (Fig. 4A), with a distribution similar to that of endogenous 5*S* in the same cell type (*18*). After application of 600 mM sucrose, a form of cellular stress that induces the formation of cytoplasmic RNA granules (*19*), 5*S*-Spinach relocalized to large (~2 to 3 μm) cytosolic foci, many of which colocalize with T-cell intracellular antigen-1–related protein (TIAR), a marker of stress granules (fig. S7) (*20*).

To monitor live-cell 5*S* dynamics, cells were treated with the Pol III inhibitor ML-60218 (*21*), which reduces 5*S*-Spinach fluorescence to baseline levels (movie S1). We first monitored nuclear export of 5*S*-Spinach. After washout of ML-60218, cells were incubated with leptomycin B, an inhibitor of nuclear export of 5*S* (*22*). Under these conditions, 5*S*-Spinach accumulates in the nucleus. Upon removal of leptomycin-B, 5*S*-Spinach rapidly appeared in the cytosol (movie S1), indicating highly efficient nucleocytoplasmic trafficking of 5*S*. We next monitored the induction of 5*S*-Spinach in response to sucrose. After washout of ML-60218, treatment of cells with sucrose resulted in rapid induction of 5*S*-Spinach over 60 min and a higher total level of 5*S*-Spinach than that in untreated cells (Fig. 4B and movie S2). Unlike control cells, sucrose treatment caused 5*S*-Spinach to accumulate to higher levels in the nucleus than in the cytosol (fig. S8), possibly reflecting saturation of the nuclear export machinery. Additionally, 5*S*-Spinach accumulated in cytoplasmic granular structures 30 min after sucrose treatment, which is consistent with stress granule formation (movie S2). We next examined the time course of relocalization of 5*S*-Spinach into granules in cells not treated with ML-60218. Before experimental treatment, 5*S*-Spinach exhibited diffuse nuclear and cytoplasmic localization (Fig. 4C). After sucrose treatment, 5*S*-Spinach clustered into granules in as little as 9 min (movie S3), with new granules continuing to form up to 30 min later. Together, these data indicate the

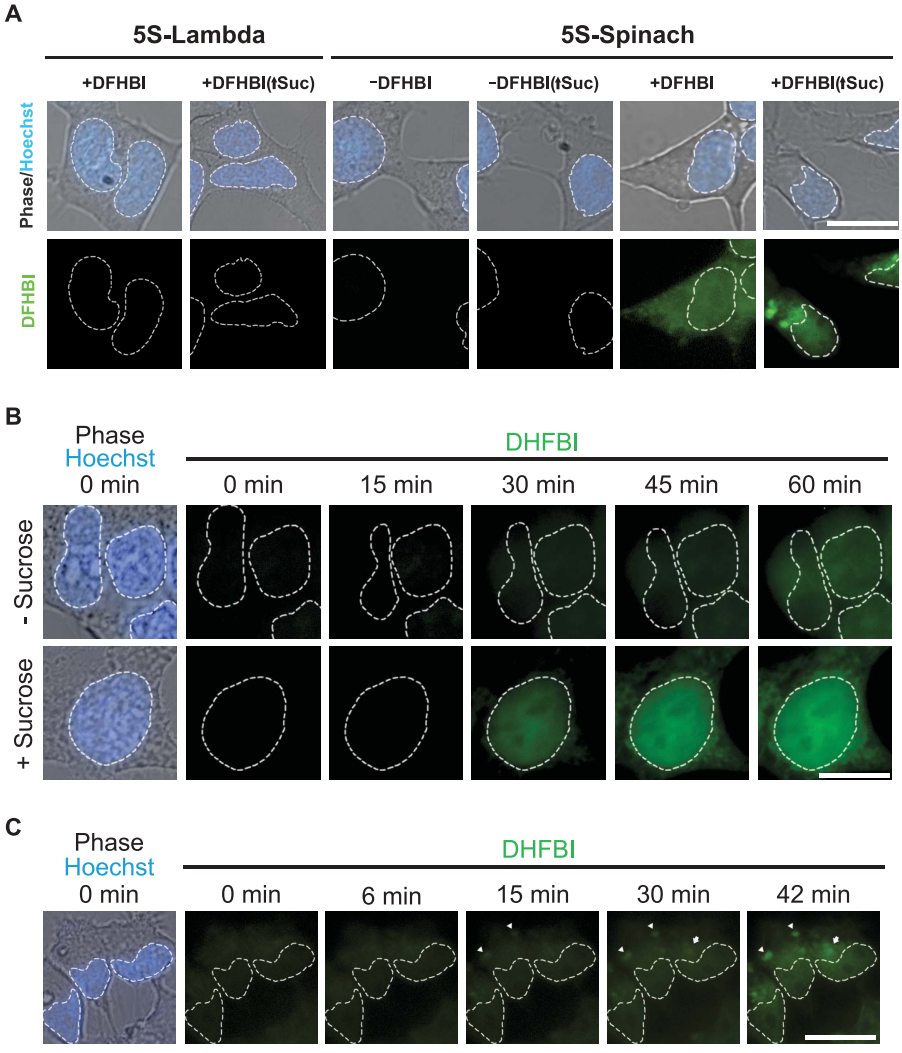

Fig. 4. Live-cell imaging of Spinach fusion RNAs. (**A**) Live-cell imaging of Spinach-tagged 5*S* RNA. Fluorescence and phase images of HEK293 T cells expressing 5*S* tagged with either Spinach or Lambda, a control RNA. Fluorescence is detected in 5*S*-Spinach–expressing cells in the presence of 20 μM DFHBI, with granule formation present in cells treated with 600 mM sucrose for 30 min (↑Suc). White dashed lines indicate nuclear borders assessed by means of Hoescht 33342 staining. (**B**) 5*S*-Spinach RNA induction in response to stress. 5*S*-Spinach–expressing HEK293 T cells were pretreated with 30 nM ML-60128 for 16 hours and then treated with vehicle or 600 mM sucrose for 60 min. Treatment of cells with sucrose resulted in a rapid induction of 5*S*-Spinach RNA and an increase in total 5*S*-Spinach levels compared with control cells. (**C**) 5*S*-Spinach RNA localization into granules. 5*S*-Spinach–expressing HEK293 T cells were stimulated with 600 mM sucrose in order to monitor the rate of formation of 5*S*-Spinach–containing granules. Arrowheads indicate granules that formed earliest, and arrows indicate granules that developed later during the time course of treatment. Scale bar, 10 μm.

ability of Spinach to reveal the intracellular dynamics of RNA in living cells.

We have described a palette of RNA-fluorophore complexes spanning much of the visible spectrum. RNAs can be tagged with Spinach, providing a simple strategy for introducing a compact fluorescent tag for live-cell imaging of RNAs while avoiding the problems associated with current methods for tagging RNAs (*23*). Spinach is different from GFP in that it exhibits considerable resistance to photobleaching, and fluorescence is observed shortly after Spinach transcription in cells, which contrasts with the delay in acquisition of fluorescence by nascent GFP because of the requirement for fluorophore maturation (*24*). The results described here raise the possibility of using genetically encoded RNA-fluorophore complexes for other applications, including RNA-RNA and RNA-protein fluorescence resonance energy transfer, and simultaneous imaging of multiple RNAs.

References and Notes

1. D. M. Chudakov, M. V. Matz, S. Lukyanov, K. A. Lukyanov, *Physiol. Rev.* **90**, 1103 (2010).
2. H. Niwa *et al.*, *Proc. Natl. Acad. Sci. U.S.A.* **93**, 13617 (1996).
3. W. W. Ward, S. H. Bokman, *Biochemistry (Mosc.)* **21**, 4535 (1982).
4. S. R. Meech, *Chem. Soc. Rev.* **38**, 2922 (2009).
5. J. R. Babendure, S. R. Adams, R. Y. Tsien, *J. Am. Chem. Soc.* **125**, 14716 (2003).
6. T. P. Constantin *et al.*, *Org. Lett.* **10**, 1561 (2008).
7. C. Szent-Gyorgyi *et al.*, *Nat. Biotechnol.* **26**, 235 (2008).
8. J. C. Liao, J. Roider, D. G. Jay, *Proc. Natl. Acad. Sci. U.S.A.* **91**, 2659 (1994).
9. A. D. Ellington, J. W. Szostak, *Nature* **346**, 818 (1990).
10. C. Tuerk, L. Gold, *Science* **249**, 505 (1990).
11. M. Zuker, *Nucleic Acids Res.* **31**, 3406 (2003).
12. Materials and methods are available as supporting material on *Science* Online.
13. R. Heim, A. B. Cubitt, R. Y. Tsien, *Nature* **373**, 663 (1995).
14. R. Y. Tsien, *Annu. Rev. Biochem.* **67**, 509 (1998).
15. N. C. Shaner *et al.*, *Nat. Biotechnol.* **22**, 1567 (2004).
16. A. F. Bell, X. He, R. M. Wachter, P. J. Tonge, *Biochemistry* **39**, 4423 (2000).
17. L. Ponchon, F. Dardel, *Nat. Methods* **4**, 571 (2007).
18. C. P. Paul *et al.*, *Mol. Ther.* **7**, 237 (2003).
19. M. G. Thomas, M. Loschi, M. A. Desbats, G. L. Boccaccio, *Cell. Signal.* **23**, 324 (2011).
20. N. L. Kedersha, M. Gupta, W. Li, I. Miller, P. Anderson, *J. Cell Biol.* **147**, 1431 (1999).
21. L. Wu *et al.*, *Eukaryot. Cell* **2**, 256 (2003).
22. K. Murdoch, S. Loop, F. Rudt, T. Pieler, *Eur. J. Cell Biol.* **81**, 549 (2002).
23. S. Tyagi, *Nat. Methods* **6**, 331 (2009).
24. R. Heim, D. C. Prasher, R. Y. Tsien, *Proc. Natl. Acad. Sci. U.S.A.* **91**, 12501 (1994).

Acknowledgments: We thank M. S. Cohen, A. Deglincerti, J. D. Warren, and S. C. Blanchard (Weill Cornell Medical College) and D. S. Tan (Sloan-Kettering Institute) for useful comments and suggestions; D. Engelke (University of Michigan) for providing plasmids containing the 5*S* sequence; and F. Dardel (Université Paris Descartes) for providing plasmids containing the tRNA scaffold sequence. This work was supported by the McKnight Neuroscience Technology Innovation Award, Weill Cornell Medical College, and National Institute of Neurological Disorders and Stroke grant NS064516 (S.R.J.) and training grant T32CA062948 (J.S.P.).

Supporting Online Material

www.sciencemag.org/cgi/content/full/333/6042/642/DC1
Materials and Methods
SOM Text
Figs. S1 to S8
Table S1
References (*25*–*40*)
Movies S1 to S3

21 April 2011; accepted 16 June 2011
10.1126/science.1207339

Isolation of Succinivibrionaceae Implicated in Low Methane Emissions from Tammar Wallabies

P. B. Pope,[1,2] W. Smith,[1] S. E. Denman,[1] S. G. Tringe,[3] K. Barry,[3] P. Hugenholtz,[3,4] C. S. McSweeney,[1] A. C. McHardy,[5,6] M. Morrison[1,7]*

The Tammar wallaby (*Macropus eugenii*) harbors unique gut bacteria and produces only one-fifth the amount of methane produced by ruminants per unit of digestible energy intake. We have isolated a dominant bacterial species (WG-1) from the wallaby microbiota affiliated with the family Succinivibrionaceae and implicated in lower methane emissions from starch-containing diets. This was achieved by using a partial reconstruction of the bacterium's metabolism from binned metagenomic data (nitrogen and carbohydrate utilization pathways and antibiotic resistance) to devise cultivation-based strategies that produced axenic WG-1 cultures. Pure-culture studies confirm that the bacterium is capnophilic and produces succinate, further explaining a microbiological basis for lower methane emissions from macropodids. This knowledge also provides new strategic targets for redirecting fermentation and reducing methane production in livestock.

Kangaroos and wallabies possess adaptations to herbivory that include a forestomach supporting a cooperative host-microbe association that releases nutrients from plant biomass. The structure-function relationships inherent to these microbiomes have only recently been examined, in part because of their capacity for lignocellulose degradation coupled with low methane production, relative to domesticated livestock (*1*, *2*). The differences in methane emissions between the macropodids and ruminants may be partially explained by the anatomical differences between the host animals, with the macropodid digestive system resulting in shorter retention time of particulate digesta within the foregut, which might prevent the establishment of methanogenic archaea (*3*). Methanogenic archaea have since been found in the foregut microbiomes of the Tammar wallaby (*Macropus eugenii*) and the eastern grey kangaroo (*M. giganteus*), albeit at lower levels than those found in ruminants (*4*). Functional gene analyses and limited cultivation studies have also suggested the presence of clades of acetogenic bacteria in the macropodid foregut (*5*, *6*). Metagenomic analysis revealed that the foregut microbiome of the Tammar wallaby varies seasonally but is principally composed of bacteria belonging to the phyla Firmicutes, Bacteroidetes, and Proteobacteria, with the majority of the observed phylotypes only distantly related to cultivated species (*7*). Approximately 77% of the recovered Proteobacteria sequences [representing 9% of all sequences recovered in the 16*S* ribosomal RNA (rRNA) clone library] were assigned to just two deeply branched operational taxonomic units within the family Succinivibrionaceae; hereafter referred to as Wallaby Group 1 (WG-1; table S1 and fig. S1).

The closest cultured relatives of WG-1 all belong to the family Succinivibrionaceae, which includes *Succinivibrio, Ruminobacter*, and *Anaerobiospirillum* spp., although WG-1 does not share more than 93% sequence identity to the 16*S* rRNA genes of any of these described species. Members of the Succinivibrionaceae produce succinate as their principal fermentation end product, and for some exogenous sources of hydrogen stimulate succinate formation (*8*). If WG-1 possesses the same metabolic characteristics, the bacterium might underpin a fermentation scheme that helps to explain the low methane phenotype attributed to the macropodids. To examine the contributions of WG-1 to fermentation in the macropodid foregut requires its isolation, preferably in axenic culture. A combination of data sets (*7*) and a nucleotide composition–based binning algorithm (PhyloPythia) was used to isolate and characterize a strain representing the WG-1 lineage. PhyloPythia uses a multiclass support vector machine classifier for the taxonomic assignment of variable-length metagenome

[1]CSIRO Livestock Industries, Queensland Bioscience Precinct, St Lucia 4067, Australia. [2]Department of Chemistry, Biotechnology and Food Science, Norwegian University of Life Sciences, Ås 1432, Norway. [3]United States Department of Energy, Joint Genome Institute, Walnut Creek, CA 94598, USA. [4]Australian Centre for Ecogenomics, School of Chemistry and Molecular Biosciences and Institute for Molecular Bioscience, St Lucia 4072, Australia. [5]Max Planck Research Group for Computational Genomics and Epidemiology, Max Planck Institute for Informatics, Campus E1 4, 66123 Saarbrücken, Germany. [6]Department for Algorithmic Bioinformatics, Heinrich-Heine University Düsseldorf, 40225 Düsseldorf, Germany. [7]Department of Animal Sciences, Ohio State University, Columbus, OH 43210, USA.

*To whom correspondence should be addressed. E-mail: mark.morrison@csiro.au